Icarus 318 (2019) 14–21

Contents lists available at ScienceDirect

Icarus

journal homepage: www.elsevier.com/locate/icarus

The spectral parameter maps of Ceres from NASA/DAWN VIR data

A. Frigeri[a,*], M.C. De Sanctis[a], E. Ammannito[b], F. Tosi[a], M. Ciarniello[a], F. Zambon[a], F.G. Carrozzo[a], A. Raponi[a], T. McCord[c], C.A. Raymond[d], C.T. Russell[e]

[a] Istituto Nazionale di Astrofisica (INAF), Istituto di Astrofisica e Planetologia Spaziali (IAPS), Via Fosso del Cavaliere n. 100, 00133, Rome, Italy
[b] Italian Space Agency (ASI), Rome, Italy
[c] Bear Fight Institute, Winthrop, WA, USA
[d] Jet Propulsion Laboratory, California Institute of Technology, CA, Pasadena, USA
[e] Institute of Geophysics and Planetary Physics, University of California, CA, Los Angeles, USA

ARTICLE INFO

Article history:
Received 30 April 2017
Revised 19 December 2017
Accepted 16 April 2018
Available online 22 April 2018

Keywords:
Remote sensing
Spectroscopy
Ceres
NASA/Dawn
GIS

ABSTRACT

This article presents the spectral parameter maps used in this Surface Composition of Ceres Special Issue. The definition and use of spectral parameters has always played a fundamental role in understanding the properties and composition of a planetary surface. Mapping proper spectral parameters shows the global mineralogical diversity across Ceres. In this work, we discuss the production process of Ceres spectral parameter maps derived by the data of the Visible and Infrared mapping spectrometer (VIR) onboard NASA's Dawn mission. We describe the data processing of the VIR spectra and the procedure to retrieve the geometries (latitude, longitude and illumination angles) of the acquired data. Spectra and geometries are used to project and mosaic this data to produce Geographic Information System-compatible spectral parameters maps of Ceres. An overview of the variability of the data across the quadrangles is given, addressing the specific analysis to each quadrangle mapping paper included in this special issue.

1. Introduction

The knowledge of the mineralogical composition of the surface of a planetary body or an asteroid represents an important element in understanding its origin and geological evolution. Since the 1970s, ground-based and spaceborne reflectance spectroscopy unveiled the mineralogical composition of planetary surfaces of terrestrial planets and asteroids. Between March 2015 and November 2016, NASA's Dawn mission (Russell et al., 2016) acquired remote sensing data of Ceres from five different orbital phases defined by the altitude of the spacecraft from the surface: Survey phase (~4400 km altitude), two High Altitude Mapping Orbit phases (HAMO and XMO2, ~1500 km altitude), and two Low Altitude Mapping Orbit phases (LAMO and XMO1, ~378 km altitude) (Russell et al., 2013). Imagery, elemental information and hyperpectral data were returned by the instruments of Dawn's payload, respectively: the Framing Camera (FC, Sierks et al., 2011), the Gamma Ray and Neutron Detector (GRaND, Prettyman et al., 2011) and the Visible and InfraRed spectrometer (VIR, De Sanctis et al., 2011).

From these experiments, we had the opportunity to collect data of unprecedented quality and spatial resolution to expand our knowledge about Ceres's geologic history, through its shape and surface composition.

From the four orbit phases, Dawn's Visible and Infrared Mapping Spectrometer (VIR) acquired spectra in the range of wavelengths between 0.25 and 5.1 μm with a spatial resolution reaching about 100 m/pixel during the LAMO phase. Reflectance spectra in the visible and infrared range acquired by VIR carry many of the information on the mineralogy of the area being observed by the instrument. However, they are also affected by instrumental artifacts and illumination conditions, so that a direct conversion from spectra to single mineral abundances is tricky and generally made on a limited number of spectra, before performing a proper data reduction. Studies on the comparison of spectra from remote sensed data and from the laboratory allow for synthesizing spectral parameters or indexes for each spectra. Different spectral parameters can be combined to detect specific physical and compositional states of the observed surface.

The average spectrum of Ceres shows several absorption bands within the 2.6 to 4.2 μm region, including those typical of H_2O and OH^- bearing minerals. The carbonaceous chondrites and other hydrated ammoniated and carbonate material exhibit absorption in the same range, although the overall spectra are different from the one detected from the surface of Ceres. The best fit of laboratory

* Corresponding author.
E-mail address: alessandro.frigeri@iaps.inaf.it (A. Frigeri).

https://doi.org/10.1016/j.icarus.2018.04.019
0019-1035/

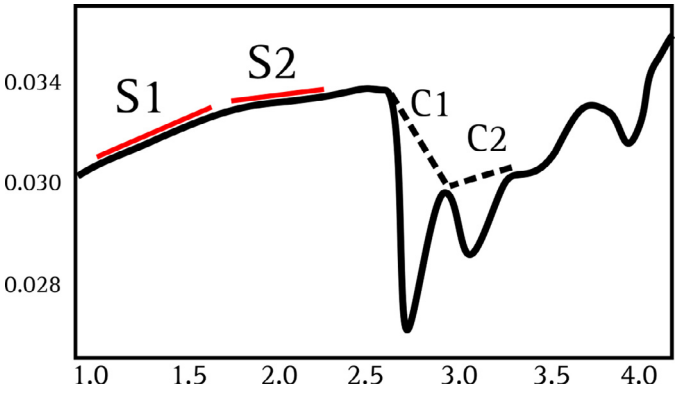

Fig. 1. Extraction of spectral parameters from VIR spectra. C1 and C2 are the continuums which are subtracted from the spectra to extract the band depths. S1 and S2 are the two spectral slopes. See the text for exact wavelengths values for band depths and slope computations.

sample spectra with the ones acquired by VIR is given by smectite clays, in particular NH_4-montmorillonite, and other mineralogical phases, such as antigorite, Mg-carbonate, and a dark component (De Sanctis et al., 2015).

Although Ceres mineralogy is dominated by clays, several localized areas rich in sodium carbonates are found in bright spots, called *faculae* in official nomenclature (Carrozzo et al., 2018).

The VIR mapping spectrometer has been critical for outlining the geologic characteristics of bright spots, and faculae on Ceres. In the work of De Sanctis et al. (2016), the mineralogical analysis shows that the faculae are mainly made up of sodium carbonates with some ammonium chlorides and alluminium phyllosilicates. Spectral parameters extracted by the typical absorption bands of these mineralogical species are particularly useful in mapping their relative abundances on Ceres.

The process of mapping those single spectral parameter values over large areas from an orbital platform enable the observation of the spatial variation of the mineralogy across the dwarf planet.

Within this surface composition of Ceres special issue (McCord and Zambon, this issue), here we describe the development of the spectral parameter maps of Ceres.

2. Spectral parameters for the mineralogical mapping of Ceres

While at Vesta we produced pyroxene-related spectral parameters (Frigeri et al., 2015), on Ceres we extract several spectral parameters connected to different mineralogical aspects. In this Special Issue, we concentrate on mapping the variation of these parameters retrieved by VIR data acquired during the HAMO phase (spatial resolution ~380 m/pixel), filling coverage gaps with data from Survey phase (resolution ~1100 m/pixel). Data at those resolution enable regional studies on the dwarf planet Ceres.

The work of Ammannito et al. (2016) shows that phyllosilicate-related band centers do not vary across Ceres, but rather that there is a variation in their band depths at 2.7 and 3.1 μm. In general, band depths are difficult to interpret unequivocally as they are related to several factors, such as the abundance of a particular species, the amount of opaque materials in the mixture, or the size of the material's grains (Clark, 1999).

Other parameters we present in this paper are two spectral slopes, respectively between 1.163 and 1.891 μm and 1.891 and 2.250 μm.

Spectral slope variations are associated with terrain's maturity and can also provide information on the grain size (Clark et al., 1993; Clark, 1999; Stephan et al., 2017).

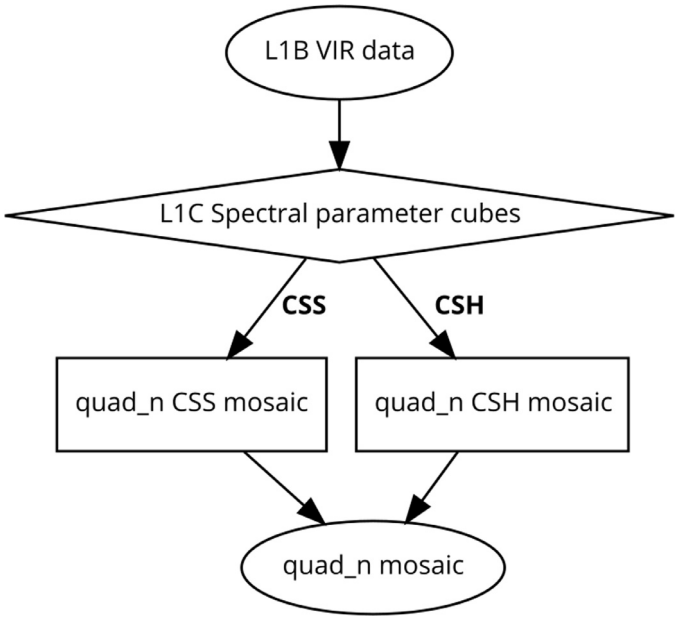

Fig. 2. The code flow used for the development of the spectral parameter's quadrangle maps. CSS and CSH mosaics in the specific quadrangle's coordinate reference system are produced separately and then combined in the final map.

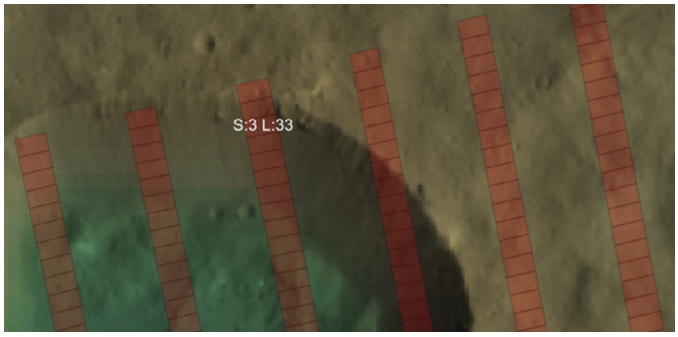

Fig. 3. The geometric model for VIR data. VIR data cube 493300377 geometry projected over an altitude-colorized FC image mosaic. The red ribbons are single-acquisition slits, or data lines. Sample 3 of line 33 is highlighted. The slits are spatially separated because of the relative speed of the spacecraft and the integration time typical of the lower orbits. (For interpretation of the references to color in this figure legend, the reader is referred to the web version of this article.)

Lower spectral slope values are often associated with young terrains whereas higher spectral slope values are typical of older terrains (Nettles et al., 2011; Stephan et al., 2017).

We have also considered albedo at wavelengths of 1.2 μm and 1.9 μm, which give global spatial distribution of the albedo measured by VIR at these two wavelengths.

3. Data and methods

The VIR spectrometer delivers data frames, or cubes, organized into spatial lines and pixels and hyperspectral data into 864 bands from two detectors, one in the visible (from 0.25 to 1.07 μm) and the other in the infrared range (from 0.95 to 5.1 μm), with spectral sampling of 1.8 nm and 9.8 nm, respectively (De Sanctis et al., 2011). The spatial resolution depends on the altitude of the mapping orbit chosen in the planning phase. At the most distant mapping orbit phase, the spatial resolution is about 700 m, reaching less than 100 m per pixel in the LAMO phase.

The spectral parameters maps are computed starting from the radiometrically calibrated VIR data products. Interactive Data Lan-

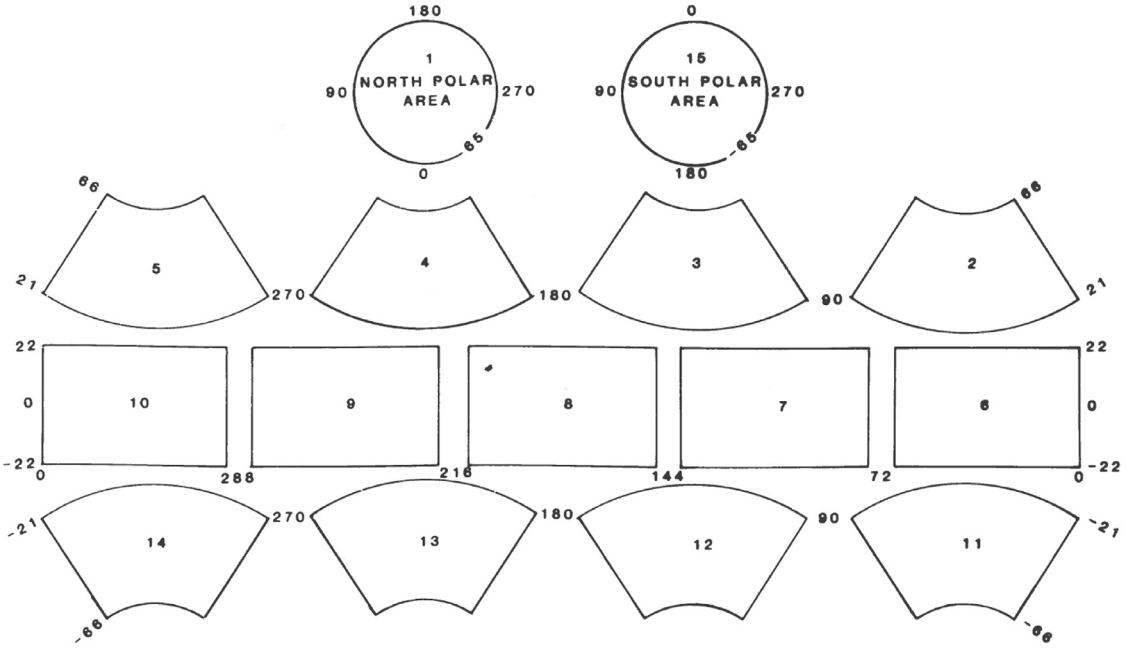

Fig. 4. For the mineralogic mapping of Ceres we use this 15-quadrangle scheme, as suggested by Greeley and Batson (1990) for middle-sized bodies, similar to what has been adopted for the Imagery Atlas of Vesta and Ceres (Roatsch et al., 2012, 2016) and the Geologic Mapping of Vesta and Ceres (Williams et al., 2014, 2017).

guage (IDL) scripts have been developed within the VIR team in order to generate an archive of spectral parameter data cubes (De Sanctis et al., 2013; Ammannito et al., 2013). The spectral parameters cubes have the same pixel and line dimensions as the original data cubes of VIR, thus every cube corresponds to a single VIR-archived data-product. For this special issue, we present a selection of cubes from Survey (Ceres Science Survey, CSS) and the HAMO (Ceres Science Hamo, CSH) phases. The list of data cubes selected for the production of the maps presented in this work is reported in the online supplementary material.

For every cube, an auxiliary geometric cube is generated using Spacecraft Planet Instrument C-matrix Events (SPICE) (Acton, 1999) and specific IDL software. The physical footprint for each integration interval is generated, taking into account the spacecraft orientation, the instrument pointing and the shape of the asteroid. This information is used to build the geometric model of the footprints within a Geographic Information System (GIS). The georeferenced data represent the base for the production of mosaics.

3.1. Spectral data processing

VIR data are stored in the form of digital data cubes with a Planetary Data System (PDS) version 3 label (De Sanctis, 2012). Spectral parameters are computed from calibrated VIR data after applying a despike algorithm, the removal of the thermal emission (Raponi et al., 2016) (Raponi, 2017, this issue) and a proper photometric correction (Ciarniello et al., 2017). The spectral parameters are finally put into multi-band data cubes.

Band depths at 2.7 and 3.1 μm are computed after removing the continuum as depicted in Fig. 1. Continuum C1 is the straight line between the reflectance at 2.63 μm and the local maximum value between 2.91 μm and 3.01 μm. Continuum C2 is the straight line between the maximum reflectance in the range 2.91–3.01 μm and 3.19–3.24 μm.

The band depths have been computed as defined by Clark and Roush (1984):

$$D_b = \frac{R_c - R_b}{R_c} \quad (1)$$

where R_b is the reflectance at the band center and R_c is the reflectance of the continuum at the band center.

Spectral slopes are computed as follows (Cuzzi et al., 1999; Filacchione et al., 2012):

$$S = \frac{R_{\lambda_1} - R_{\lambda_0}}{R_{\lambda_1}(\lambda_1 - \lambda_0)} \quad (2)$$

where R_{λ_i} is the reflectance at the wavelength λ_i.

This special issue uses two spectral slopes, named S1 and S2. S1 uses λ_0 of 1.163 μm and λ_1 of 1.891 μm, while S2 is computed with λ_0 of 1.891 μm and λ_1 of 2.250 μm (see S1 and S2 in Fig. 1).

3.2. Geoprocessing

Geometric information are computed using the latest version of the SPICE toolkit (Acton, 1999), which includes the shape model of Ceres relative to the HAMO phase of the mission, released by the Deutsches Zentrum für Luft und Raumfahrt (DLR) (Preusker et al., 2015). The acquisition geometries are stored as data cubes that are used to create the instrument's footprints.

The final maps have been produced using the Free Open Source software tools available from the OSGeo software stack (Hall and Leahy, 2008). In particular for this work we have combined the mosaicking capabilities of Integrated Software for Imagers and Spectrometers (ISIS) version 3 and the robust geospatial processing environment offered by the Geographic Information System (GIS) engine the Geographical Resources Analysis Support System (GRASS), which includes more than 350 modules for managing, analyzing and displaying geospatial data (Neteler et al., 2012).

The use of GIS data models allows for handling the multi-resolution data coming from the different orbital ranges of the

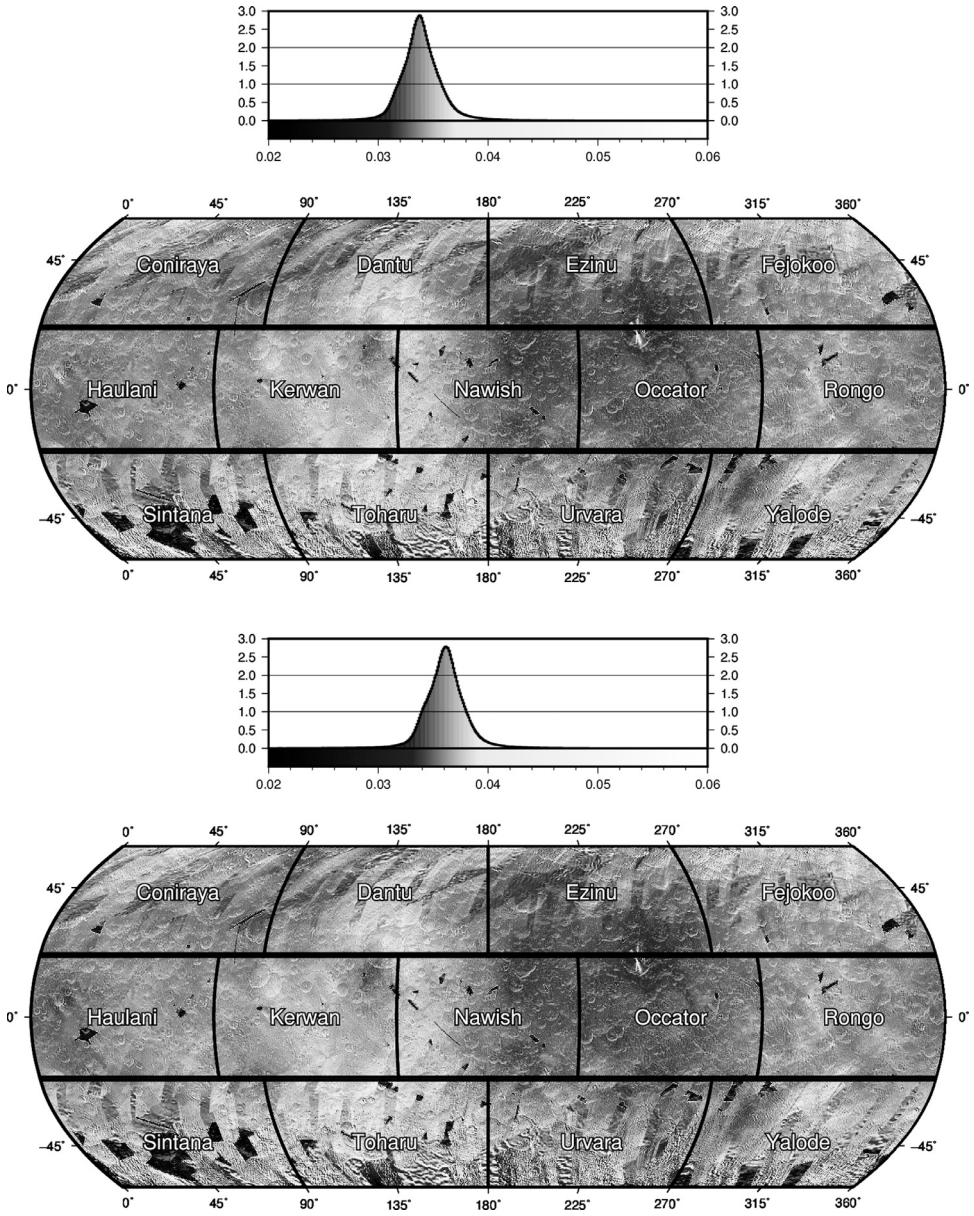

Fig. 5. Top: albedo map at 1.2 μm (*Albedo I*). Bottom: albedo map at 1.9 μm (*Albedo II*).

mapping campaign of Dawn at Ceres and mosaicking these data into the quadrangle maps, following the flow reported in the diagram of Fig. 2.

Since the observation of the variation of spectral parameters within its morphologic context is extremely important, we decided to map the spectral parameters with a final spatial resolution of 140 m per pixel. Thus we used the Survey (Ceres Science Survey, CSS) and HAMO (Ceres Science HAMO, CSH) data, keeping the final resolution similar to the imagery (35 m per pixel for the LAMO image mosaic) and topographic maps (60 m per pixel) made available by the Framing Camera Team.

Fig. 3 shows the geometric data model of VIR data used to produce the spectral parameters maps. Note that consecutive ground swaths of VIR footprints are separated. This is due to the particular mission design of Dawn, in which we must take into account the combination of integration time and spacecraft velocity in projecting the slit data on the surface. For the case of the HAMO and LAMO orbits, the relative ground-spacecraft speed is particularly high, requiring an accurate representation of the instrument's footprints. A smearing effect is taken into account by considering full integration times of the slits instead of instantaneous field of view of the timestamp corresponding to a particular slit.

In order to produce maps from the single observations, we mosaicked the data using average overlapping values.

The final spatial resolution of the maps has been set to 140 m per pixel, which is four times the spatial resolution of the most detailed image mosaic from the FC.

Spectral parameters maps are thus produced at a resolution of 140 m per pixel within the GIS environment and exported as Geotiff and ENVI-formatted files, following a 15-tile quadrangle scheme (Fig. 4) commonly used for medium-sized planetary bodies (Greeley and Batson, 1990), and matching the Framing Camera Atlas of Vesta and Ceres (Roatsch et al., 2012).

A graphic rendition of the spectral parameters has been produced as images from the GIS data, along with the addition of a shaded relief obtained from the digital terrain model (DLR) (Jaumann et al., 2012) and the official International Astronomical Union (IAU) nomenclature. This visualization allows for the identi-

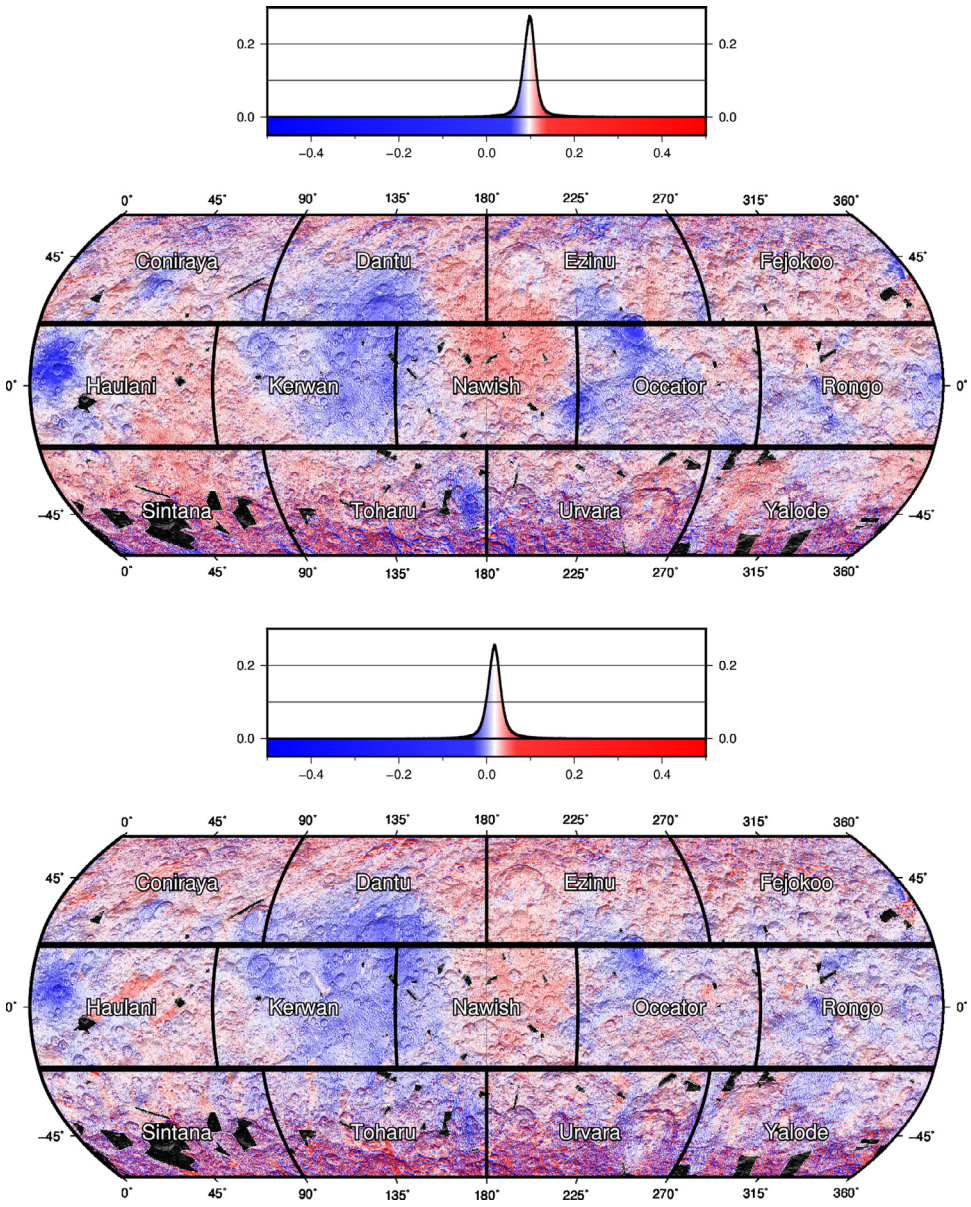

Fig. 6. Top: Slope I, the spectral slope between 1.163 μm and 1.891 μm (S1). Bottom: Slope II, the spectral slope between 1.891 μm and 2.250 μm (S2).

fication of the general morphologic setting and correlation of the mineralogy to the main topographic features of every quadrangle.

3.3. The geographic framework and the tiling scheme

For Ceres, NASA's Dawn mission adopts a planetographic coordinate system, with positive east longitudes, over a spherical reference surface with a radius of 470 km. The prime meridian is anchored to the 400-m diameter Kait crater (Raymond and Roatsch, 2015).

In order to produce usable cartographic products, we followed the tiling scheme suggested for medium-sized planetary bodies (Greeley and Batson, 1990). Within this scheme, the Mercator projection is used for quadrangles of the equatorial area, while the Lambert projection is used for northern and southern quadrangles, and the stereographic projection is used for polar regions (Fig. 4).

This is the same tiling scheme used for the production of the atlas of Ceres. This, together with the use of georeferenced GIS files, encourages the interchange of files among the team, facilitating comparative studies of different high-level data products derived from different instruments.

4. The spectral parameter maps

The spectral parameter maps have been projected following the tiling scheme described above (depicted in Fig. 4), formatted into a GIS- and ENVI-compatible format, and distributed to the lead authors of this mineralogical mapping issue.

In order to have an overview on the diversity of these parameters across Ceres, we present herein the spectral parameter data merged in a Robinson projection which allows for a global view. Maps are cut at ± 60° because spectral parameter data are particularly noisy at higher latitudes due to the adverse illumination conditions. Ceres inclination axis also affects the illumination angles between the northern and the southern quadrangles, where the signal-to-noise ratio of spectra and thus the parameters' maps is lower.

The six spectral parameter maps are reported in Figs. 5–7. Each map displays also the color-scale between minimum and maxi-

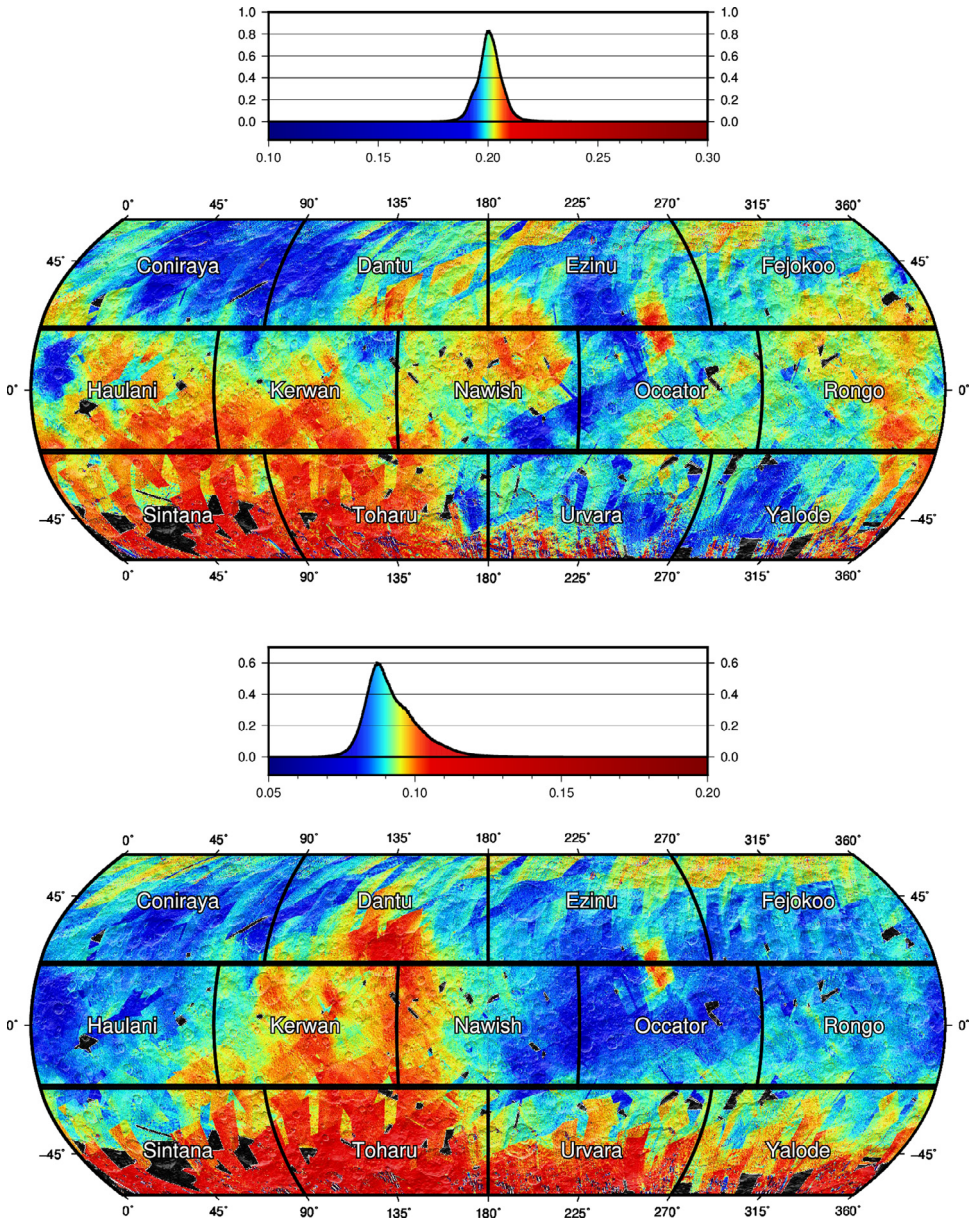

Fig. 7. Top: Band Depth I, the band depth at 2.7 µm. Bottom: Band Depth II, the band depth at 3.1 µm.

mum values and the frequency distribution of the data represented as a histogram.

Albedo I map at 1.2 µm (Fig. 5-top) shows high values on quadrangles Dantu, Kerwan, Nawish and Thoaru crossing longitude 135°. Low values are concentrated in the eastern sector of Nawish and at the Occator/Ezinu border, where the Occator crater (92 km) is located, showing a large albedo variation within its floor. The histogram is symmetric and unimodal.

Globally, the spatial distribution of albedo in the *Albedo I* map (1.2 µm, Fig. 5-top) follows the trend of the *Albedo II* map (1.9 µm, Fig. 5-bottom).

The map shown in Fig. 6 exhibits concentrated lower slope values corresponding to the Haulani (Tosi et al., 2017) and Occator (Longobardo et al., 2017) big craters, Ahuna Mons in the Rongo quadrangle (Zambon et al., 2016; 2017) and around the Juling and Kupalo craters in the Toharu quadrangle (De Sanctis et al., 2017). The same trend is recognizable in the slope II map of Fig. 6.

The map of band depth I in Fig. 7 shows that southwestern quadrangles have an overall higher 2.7 µm band depth. Within these quadrangles, Haulani crater shows a contrasting lower value in its surroundings. Within Nawish, the Heneb crater floor has low values, while its related ejected materials are high in value.

The band depth II map in Fig. 7 has a slightly different trend when compared with the band depth I map. Southern quadrangles have higher values, as well as the quads crossing the 135-degree meridian. The Haulani quadrangle does not show big variations, different from what is observed in band depth I. In west of Occator, an area with deeper values of band 3.1 µm is evident. The band depth II map shows a right-skewed histogram indicating a global predominance of shallower band depths over deeper ones.

Table 1 summarizes the main features found by lead authors of the mineralogical mapping papers included in this issue and discussed in detail in the single articles within this special issue.

Table 1
The Ceres quadrangles mapped in this issue by various authors with main mineralogic features.

Quad	Quad name	Reference	Highlights
Ac-H-02	Coniraya	A. Raponi	Aliphatics compounds in Ernutet area, Na-carbonates in Ikapati crater.
Ac-H-03	Dantu	Katrin Stephan	Dantu crater, located in a huge depression named Vendimia Planitia, which possibly represents a completely degraded impact basin formed in the beginning of Ceres' geological history. Most parts of this depression are characterized by strong phyllosilicate absorptions, which are stronger than elsewhere on Ceres' surface.
Ac-H-04	Ezinu	J.-Ph. Combe	Largely homogenous surface, except small, high-albedo carbonate-rich areas, and one zone on dark, lobate materials on the floor of Occator.
Ac-H-05	Fejokoo	S. Singh	Bright material rich in hydroxylated material, with high values of both the 2.7 and 3.1 μm band depth.
Ac-H-06	Haulani	F. Tosi	Bluest visible to near-infrared spectral slope in Haulani crater floor and ejecta, associated with substantial decrease of OH- and NH_4-bearing minerals.
Ac-H-07	Kerwan	Palomba	Phyllosilicates and ammoniated clays generally are correlated in the Kerwan quadrangle, even if departure from this behavior is observed in the floor of Kerwan, Inamahari and Homsuk craters. The greatest abundance of NH_4-phyllosilicates is found in Rao and Kerwan ejecta, while Bonsu and Tafakula floors are the most depleted in volatile, as well as Inamahari and Dantu ejecta.
Ac-H-08	Nawish	G. Carrozzo	NH_4-phyllosilicates dichotomy is present between the eastern and the western side of the quadrangle.
Ac-H-09	Occator	A. Longobardo	The major features observed in the Occator quadrangle are the occurrence of Na-carbonates in the younger terrains of Cerealia and Vinalia faculae and Azacca crater.
Ac-H-10	Rongo	F. Zambon	Na-carbonates rich areas in Ahuna Mons flanks, Xevioso crater in Liberalia Mons, and Begbalel crater. Part of the Haulani ejecta cover the eastern side of the quadrangle, while part of Urvara and Yalode impact basin are included in the Rongo quadrangle.
Ac-H-11	Sintana	M.C. De Sanctis	Tupo and Braciaca Craters- lower 2.7 μm band intensity not corresponding to lower 3.1 band intensity
Ac-H-12	Toharu	M.C. De Sanctis	Juling and Kupalo craters-water ice in Juling and high content of Na-carbonates in Kupalo.
Ac-H-13	Urvara	A. Longobardo	The central peak of the Urvara crater shows a deep 3.1 μm band depth, indicating an ammonium enrichment.
Ac-H-14	Yalode	A. Longobardo	The cratered terrain westwards of the Yalode basin have deeper 2.7 and 3.1 μm absorption bands, probably due to less phyllosilicate depletion following the Yalode impact.

5. Conclusions

This special issue presents mineralogical quadrangle maps of Ceres. The maps are created by averaging the spectral parameter values of overlapping footprints of VIR data cubes, making it possible to appreciate the diversity of Ceres mineralogy over large areas.

The quadrangle maps have been produced by projecting the single data footprints of the spectrometer, so that the actual geometry of measurements is kept throughout the mapping process, from the projection to the mosaicking.

The final maps have a resolution of 140 m per pixel, which is also of the same order of magnitude of the digital maps produced from the mosaicking of the Framing Camera data.

Maps have been produced in GIS-compatible formats, so cartographic metadata is included in the digital maps, facilitating future studies.

Acknowledgments

This work was supported by ASI and NASA. VIR is funded by the Italian Space Agency ASI and was developed under the leadership of INAF-Istituto di Astrofisica e Planetologia Spaziali, Rome, Italy (Grant ASI-INAF n. I/004/12/1). The instrument was built by Selex-Galileo, part of the Leonardo company, Florence, Italy. The authors are grateful for the support of the Dawn science, instrument, operations, current and future working Teams.

Supplementary material

Supplementary material associated with this article can be found, in the online version, at doi:10.1016/j.icarus.2018.04.019.

References

Acton, C.H., 1999. SPICE products available to the planetary science community. In: Lunar and Planetary Institute Science Conference Abstracts. Vol. 30 of Lunar and Planetary Inst. Technical Report., p. 1233.

Ammannito, E., De Sanctis, M.C., Capaccioni, F., Teresa Capria, M., Carraro, F., Combe, J.P., Fonte, S., Frigeri, A., Joy, S.P., Longobardo, A., Magni, G., Marchi, S., McCord, T.B., McFadden, L.A., McSween, H.Y., Palomba, E., Pieters, C.M., Polanskey, C.A., Raymond, C.A., Sunshine, J.M., Tosi, F., Zambon, F., Russell, C.T., 2013. Vestan lithologies mapped by the visual and infrared spectrometer on Dawn. Meteor. Planet. Sci. 48 (11), 2185–2198. https://doi.org/10.1111/maps.12192.

Ammannito, E., De Sanctis, M.C., Ciarniello, M., Frigeri, A., Carrozzo, F.G., Combe, J.P., Ehlmann, B.L., Marchi, S., McSween, H.Y., Raponi, A., Toplis, M.J., Tosi, F., Castillo-Rogez, J.C., Capaccioni, F., Capria, M.T., Fonte, S., Giardino, M., Jaumann, R., Longobardo, A., Joy, S.P., Magni, G., McCord, T.B., McFadden, L.A., Palomba, E., Pieters, C.M., Polanskey, C.A., Rayman, M.D., Raymond, C.A., Schenk, P.M., Zambon, F., Russell, C.T., 2016. Distribution of phyllosilicates on the surface of ceres. Science 353. Aaf4279.

Carrozzo, F.G., De Sanctis, M.C., Raponi, A., Ammannito, E., Castillo-Rogez, J., Ehlmann, B.L., Marchi, S., Stein, N., Ciarniello, M., Tosi, F., Capaccioni, F., Capria, M.T., Fonte, S., Formisano, M., Frigeri, A., Giardino, M., Longobardo, A., Magni, G., Palomba, E., Zambon, F., Raymond, C.A., Russell, C.T., 2018. Nature, formation, and distribution of carbonates on Ceres. Sci. Adv. 4 (3). http://advances.sciencemag.org/content/4/3/e1701645.

Ciarniello, M., De Sanctis, M.C., Ammannito, E., Raponi, A., Longobardo, A., Palomba, E., Carrozzo, F.G., Tosi, F., Li, J.Y., Schröder, S.E., Zambon, F., Frigeri, A., Fonte, S., Giardino, M., Pieters, C.M., Raymond, C.A., Russell, C.T., 2017. Spectrophotometric properties of dwarf planet ceres from the vir spectrometer on board the dawn mission. Astron. Astrophys. 598. A130.

Clark, R.N., 1999. Spectroscopy of rocks and minerals, and principles of spectroscopy. Man. Remote Sens. 3, 3–58.
Clark, R.N., Roush, T.L., 1984. Reflectance spectroscopy: quantitative analysis techniques for remote sensing applications. J. Geophys. Res. 89 (B7), 6329–6340. https://doi.org/10.1029/jb089ib07p06329.
Clark, R.N., Swayze, G.A., Gallagher, A., 1993. Mapping minerals with imaging spectroscopy. US Geol. Survey Office Miner. Resour. Bull. 2039 (141–150). 69.
Cuzzi, J., Clark, R., Filacchione, G., French, R., Johnson, R., Marouf, E., Spilker, L., 1999. Ring particle composition and size distribution. In: Saturn from Cassini-Huygens, vol. 89. Springer, Berlin, pp. 6329–6340. 459–509. Research https://doi.org/10.1029/jb089ib07p06329.
De Sanctis, M.C., 2012. NASA/dawn VIR imaging spectrometer calibrated data (level 1b), NASA planetary data system. dataset DWNVVIR_I1B and DWNVVIR_V1B, accessed: 2015-01-22. http://sbn.psi.edu/pds/resource/dwnvvir.html.
De Sanctis, M.C., Ammannito, E., Capria, M.T., Capaccioni, F., Combe, J.P., Frigeri, A., Longobardo, A., Magni, G., Marchi, S., McCord, T.B., Palomba, E., Tosi, F., Zambon, F., Carraro, F., Fonte, S., Li, Y.J., McFadden, L.A., Mittlefehldt, D.W., Pieters, C.M., Jaumann, R., Stephan, K., Raymond, C.A., Russell, C.T., 2013. Vesta's mineralogical composition as revealed by the visible and infrared spectrometer on Dawn. Meteor. Planet. Sci. 48 (11), 2166–2184. https://doi.org/10.1111/maps.12138.
De Sanctis, M.C., Ammannito, E., Raponi, A., Marchi, S., McCord, T.B., McSween, H.Y., Capaccioni, F., Capria, M.T., Carrozzo, G., Ciarniello, M., Longobardo, A., Tosi, F., Fonte, S., Formisano, M., Frigeri, A., Giardino, M., Magni, G., Palomba, E., Turrini, D., Zambon, F., Combe, J.P., Feldmann, W., Jaumann, R., McFadden, L.A., Pieters, C.M., Prettyman, T., Toplis, M., Raymond, C.A., Russell, C.T., 2015. Ammoniated phyllosilicates with a likely outer solar system origin on (1) Ceres. Nature.
De Sanctis, M.C., Coradini, A., Ammannito, E., Filacchione, G., Capria, M.T., Fonte, S., Magni, G., Barbis, A., Bini, A., Dami, M., Ficai-Veltroni, I., Preti, G., 2011. The VIR spectrometer. Space Sci. Rev. 163, 329–369.
De Sanctis, M.C., Frigeri, A., Ammannito, E., Carrozzo, G., Ciarniello, M., Zambon, F., Tosi, F., Raponi, A., Longobardo, A., Combe, J.P., Palomba, E., Schulzeck, F., Raymond, C.A., Russell, C., 2017. Ac-h-11 Sintana and ac-h-12 toharu quadrangles: assessing the large and small scale heterogeneities of ceres surface. Icarus.
De Sanctis, M.C., Raponi, A., Ammannito, E., Ciarniello, M., Toplis, M.J., McSween, H.Y., Castillo-Rogez, J.C., Ehlmann, B.L., Carrozzo, F.G., Marchi, S., Tosi, F., Zambon, F., Capaccioni, F., Capria, M.T., Fonte, S., Formisano, M., Frigeri, A., Giardino, M., Longobardo, A., Magni, G., Palomba, E., McFadden, L.A., Pieters, C.M., Jaumann, R., Schenk, P., Mugnuolo, R., Raymond, C.A., Russel l, C.T., 2016. Bright carbonate deposits as evidence of aqueous alteration on (1) Ceres. Nature 536, 54–57.
Filacchione, G., Capaccioni, F., Ciarniello, M., Clark, R.N., Cuzzi, J.N., Nicholson, P.D., Cruikshank, D.P., Hedman, M.M., Buratti, B.J., Lunin, J.I., Soderblom, L.A., Tosi, F., Cerroni, P., Brown, R.H., McCord, T.B., Jaumann, R., Stephan, K., Baines, K.H., Flamini, E., 2012. Saturns icy satellites and rings investigated by cassiniVIMS: III radial compositional variability. Icarus 220 (2), 1064–1096.
Frigeri, A., De Sanctis, M., Ammannito, E., Tosi, F., Longobardo, A., Zambon, F., McCord, T., Combe, J., Jaumann, R., Raymond, C., et al., 2015. The spectral parameter maps of vesta from vir data. Icarus 259, 10–20.
Greeley, R., Batson, R.M., 1990. Planetary mapping. In: Greeley, R., Batson, R.M. (Eds.), Cambridge Planetary Science Series, vol. 6. Cambridge University Press, Cambridge, UK. 296.
Hall, G.B., Leahy, M.G., 2008. Open Source Approaches in Spatial Data Handling, vol. 2. Springer.
Jaumann, R., Williams, D.A., Buczkowski, D.L., Yingst, R.A., Preusker, F., Hiesinger, H., Schmedemann, N., Kneissl, T., Vincent, J.B., Blewett, D.T., Buratti, B.J., Carsenty, U., Denevi, B.W., De Sanctis, M.C., Garry, W.B., Keller, H.U., Kersten, E., Krohn, K., Li, J.Y., Marchi, S., Matz, K.D., McCord, T.B., McSween, H.Y., Mest, S.C., Mittlefehldt, D.W., Mottola, S., Nathues, A., Neukum, G., O'Brien, D.P., Pieters, C.M., Prettyman, T.H., Raymond, C.A., Roatsch, T., Russell, C.T., Schenk, P., Schmidt, B.E., Scholten, F., Stephan, K., Sykes, M.V., Tricarico, P., Wagner, R., Zuber, M.T., Sierks, H., 2012. Vesta's shape and morphology. Science 336, 687–690.
Longobardo, A., Palomba, E., Carrozzo, F., Galiano, A., Sanctis, M.D., Stephan, K., Tosi, F., Raponi, A., Ciarniello, M., Zambon, F., Frigeri, A., Ammannito, E., Raymond, C., Russell, C., 2017. Mineralogy of the occator quadrangle. Icarus. http://www.sciencedirect.com/science/article/pii/S0019103517303329.
McCord, T.B., Zambon, F. The surface composition of Ceres from the Dawn mission. Icarus, this issue.
Neteler, M., Bowman, M., Landa, M., Metz, M., 2012. GRASS GIS: a multi-purpose open source GIS. Environ. Modell. Software 31, 124–130.
Nettles, J., Staid, M., Besse, S., Boardman, J., Clark, R., Dhingra, D., Isaacson, P., Klima, R., Kramer, G., Pieters, C., et al., 2011. Optical maturity variation in lunar spectra as measured by moon mineralogy mapper data. J. Geophys. Res. 116, E9.
Prettyman, T.H., Feldman, W.C., McSween, H.Y., Dingler, R.D., Enemark, D.C., Patrick, D.E., Storms, S.A., Hendricks, J.S., Morgenthaler, J.P., Pitman, K.M., Reedy, R.C., 2011. Dawn's gamma ray and neutron detector. Space Sci. Rev. 163, 371–459.
Preusker, F., Scholten, F., Matz, K.D., Roatsch, T., Elgner, S., Jaumann, R., Joy, S.P., Polanskey, C.A., Raymond, C.A., Russell, C.T., 2015. Shape model and rotational state of dwarf planet ceres from dawn fc stereo images. Eur. Planet. Sci. Congress 10. EPSC2015–186.
Raponi, A., Ciarniello, M., Capaccioni, F., Filacchione, G., Tosi, F., De Sanctis, M.C., Capria, M.T., Barucci, M.A., Longobardo, A., Palomba, E., Kappel, D., Arnold, G., Mottola, S., Rousseau, B., Quirico, E., Rinaldi, G., Erard, S., Bockelee-Morvan, D., Leyrat, C., 2016. The temporal evolution of exposed water ice-rich areas on the surface of 67p/churyumovgerasimenko: spectral analysis. Mon. Not. R. Astron. Soc. 462. (Suppl 1), S476. https://doi.org/10.1093/mnras/stw3281.
Raponi, A., Carrozzo, F.G., Zambon, F., De Sanctis, M.C., Ciarniello, M., Frigeri, A., Ammannito, E., Tosi, F., Combe, J.-Ph., Longobardo, A., Palomba, E., Pieters, C.M., Raymond, C.A., Russell, C.T., Leyrat, C., 2017. Mineralogical mapping of Coniraya quadrangle of the dwarf planet Ceres. Icarus.
Raymond, C. A., Roatsch, T., 2015. Ceres coordinate system description. https://sbn.psi.edu/pds/resource/ceres_coord_sys_151014.pdf, accessed June 15th 2017.
Roatsch, T., Kersten, E., Matz, K.D., Preusker, F., Scholten, F., Jaumann, R., Raymond, C., Russell, C., 2012. High resolution Vesta high altitude mapping orbit (HAMO) atlas derived from Dawn framing camera images. Planet. Space Sci. 73 (1), 283–286. Solar System science before and after Gaia. http://www.sciencedirect.com/science/article/pii/S0032063312002589.
Roatsch, T., Kersten, E., Matz, K.D., Preusker, F., Scholten, F., Jaumann, R., Raymond, C.A., Russell, C.T., 2016. High resolution ceres hamo atlas derived from dawn fc images. In: EGU General Assembly Conference Abstracts. Vol. 18 of EGU General Assembly Conference Abstracts. Pp. EPSC2016–4274.
Russell, C.T., Raymond, C.A., Ammannito, E., Buczkowski, D.L., De Sanctis, M.C., Hiesinger, H., Jaumann, R., Konopliv, A.S., McSween, H.Y., Nathues, A., Park, R.S., Pieters, C.M., Prettyman, T.H., McCord, T.B., McFadden, L.A., Mottola, S., Zuber, M.T., Joy, S.P., Polanskey, C., Rayman, M.D., Castillo-Rogez, J.C., Chi, P.J., Combe, J.P., Ermakov, A., Fu, R.R., Hoffmann, M., Jia, Y.D., King, S.D., Lawrence, D.J., Li, J.Y., Marchi, S., Preusker, F., Roatsch, T., Ruesch, O., Schenk, P., Villarreal, M.N., Yamashita, N., 2016. Dawn arrives at Ceres: exploration of a small, volatile-rich world. Science 353, 1008–1010.
Russell, C.T., Raymond, C.A., Jaumann, R., McSween, H.Y., DeSanctis, M.C., Nathues, A., Prettyman, T.H., Ammannito, E., Reddy, V., Preusker, F., O'Brien, D.P., Marchi, S., Denevi, B.W., Buczkowski, D.L., Pieters, C.M., McCord, T.B., Li, J.Y., Mittlefehldt, D.W., Combe, J.P., Williams, D.A., Hiesinger, H., Yingst, R.A., Polanskey, C.A., Joy, S.P., 2013. Dawn completes its mission at 4 Vesta. Meteor. Planet. Sci. 48, 2076–2089.
Sierks, H., Keller, H.U., Jaumann, R., Michalik, H., Behnke, T., Bubenhagen, F., Büttner, I., Carsenty, U., Christensen, U., Enge, R., Fiethe, B., Gutiérrez Marqués, P., Hartwig, H., Krüger, H., Kühne, W., Maue, T., Mottola, S., Nathues, A., Reiche, K.U., Richards, M.L., Roatsch, T., Schröder, S.E., Szemerey, I., Tschentscher, M., 2011. The dawn framing camera. Space Sci. Rev. 163, 263–327.
Stephan, K., Jaumann, R., Krohn, K., Schmedemann, N., Zambon, F., Tosi, F., Carrozzo, F., McFadden, L., Otto, K., De Sanctis, M., et al., 2017. An investigation of the bluish material on Ceres. Geophys. Res. Lett. 44 (4), 1660–1668.
Tosi, F., Carrozzo, F., Zambon, F., Ciarniello, M., Frigeri, A., Combe, J.P., Sanctis, M.D., Hoffmann, M., Longobardo, A., Nathues, A., Raponi, A., Thangjam, G., Ammannito, E., Krohn, K., McFadden, L., Palomba, E., Pieters, C., Stephan, K., Raymond, C., Russell, C., 2017. Mineralogical analysis of the ac-h-6 haulani quadrangle of the dwarf planet Ceres. Icarus. http://www.sciencedirect.com/science/article/pii/S0019103517303354.
Williams, D.A., Buczkowski, D.L., Mest, S.C., Scully, J.E., Platz, T., Kneissl, T., 2017. Introduction: the geologic mapping of ceres. Icarus.
Williams, D.A., Yingst, R.A., Garry, W.B., 2014. Introduction: the geologic mapping of vesta. Icarus 244 (0), 1–12. Special Issue: The Geology of Vesta. http://www.sciencedirect.com/science/article/pii/S0019103514001183.
Zambon, F., Carrozzo, F. G., Tosi, F., Raponi, A., Ciarniello, M., Combe, J. P., De Sanctis, M. C., Thangjam, G., Nathues, A., Hoffmann, M., Longobardo, A., Stephan, K., Raponi, A., Ammannito, E., Krohn, K., McFadden, L. A., Palomba, E., Russell, C. T., Raymond, C. A., 2017. Mineralogical analysis of quadrangle ac-h-10 rongo on the dwarf planet ceres, Icarus, this special issue.
Zambon, F., Raponi, A., Tosi, F., DeSanctis, M.C., McFadden, L.A., Carrozzo, F.G., Longobardo, A., Ciarniello, M., Krohn, K., Stephan, K., Palomba, E., Pieters, C.M., Ammannito, E., Russell, C.T., Raymond, C.A., 2016. Spectral analysis of Ahuna mons from dawn mission's visible and infrared spectrometer. Geophys. Res. Lett. 44 (1), 97–104.